*Desalination and Water Treatment*
www.deswater.com

doi: 10.5004/dwt.2023.29530

295 (2023) 73–82
May

# Preparation methods of an $MoS_2$/GO photocatalyst for the oxidation of ammonia nitrogen in photoelectric microbial cells

Jing Ren[a,b], Jiyue Zhang[a], Yao Li[a], Maohua Du[a], Na Li[a], Chunxu Hao[b,*], Rui Hu[b]

[a]*School of Environment, Liaoning University, Shenyang, Liaoning Province 110036, China, emails: renjing@lnu.edu.cn (J. Ren), 346467483@qq.com (J. Zhang), 378866837@qq.com (Y. Li), 1657151925@qq.com (M. Du), 794801512@qq.com (N. Li)*
[b]*Chinese Academy for Environmental Planning (CAEP), MEP, 100041, Beijing, China, emails: haocx_caep@126.com (C. Hao), 799952447@qq.com (R. Hu)*

Received 16 September 2022; Accepted 31 March 2023

**ABSTRACT**

Photocatalytic fuel cells (PFCs) need to operate under ultraviolet light, and the application conditions are greatly limited. Therefore, developing and utilizing new systems that adsorb visible light is critical. Molybdenum disulfide ($MoS_2$) nanomaterials have wide bandgaps, strong visible light absorption capacities, and abundant catalytic active sites. In this study, the photocathode $MoS_2$/graphene oxide (GO) was prepared by coupling it with graphene oxide by using the mechanical oscillation method ($MoS_2$/GO-MO) and the hydrothermal synthesis method ($MoS_2$/GO-TH). In addition, a PFC was constructed to treat nitrogenous wastewater. According to an X-ray diffractometer and electron microscope, regarding the characterization analysis and electrochemical analysis of the materials, the system with $MoS_2$/GO-TH electrode had the best performance with the largest output voltage, the smallest ohmic loss during the reaction, the best oxidation–reduction capacity, and the highest ammonia nitrogen removal rate. The optimal removal rate might reach up to 96.0%. On this basis, the denitrification mechanism was explored, and the results revealed that oxygen in the PFC system was the decisive factor and that there were multiple plausible reaction paths during the reaction process.

*Keywords:* Photocatalytic fuel cell; $MoS_2$ nanomaterials; Hydrothermal synthesis method; Photocathode; Denitrification mechanism

## 1. Introduction

Microbial fuel cells (MFCs) are promising for removing ammonia nitrogen and generating electricity via biological denitrification. However, their low power densities limit their practical application [1]. Photocatalysis technology can use electrons ($e^-$) and holes ($h^+$) generated by solar energy to undergo oxidation–reduction reactions with pollutants in water [2]. However, under natural conditions, electrons and holes generated by light easily recombine. Therefore, effective control of the recombination of electrons and holes is essential for improving catalytic activity. Photocatalytic fuel cells (PFCs) are based on MFCs, where the electrode material is modified with a photocatalyst to achieve photocatalytic oxidation ability. Kaneko et al. [3] used $TiO_2$ film as an anode to construct a PFC for the first time. Wang et al. [4] constructed PFCs to degrade 2,4,6-trichlorophenol (TCP). Under the same condition of an initial concentration of 200 mg/L, the TCP removal rate was 79.3% in PFC, better than that of the MFC system without lighting (66.0%) or independent photocatalysis system (56.1%). In a PFC, the generation rate of electron–hole pairs is accelerated, and the recombination process is interfered with owing to the instant transfer of photoelectrons, which helps to improve the

* Corresponding author.

transformation rate of pollutants and the power generation capacity of the battery [5–7].

Recently, nitrogen removal technology with PFCs has attracted increasing attention. Wang et al. [8] used AgI/$TiO_2$-NTs as the anode to construct a PFC system to treat ammonia nitrogen wastewater. They found that under light conditions, the holes generated by the anode directly oxidized the majority of $NH_4^+$–N to $N_2$. Cheng et al. [9] constructed a photoelectric nutrient denitrification system that relied only on UV light to remove nitrogen, and similar output voltages exhibited the possibility of replacing traditional MFCs with PFCs. The scale application of PFC for nitrogen removal has bottleneck problems, namely, a shortage of electric energy output and a lack of solar light-responsive electrode materials. According to the operating principle of a PFC, the catalytic activity of the electrode is the primary factor restricting its electricity generation performance [10]. Researchers have attempted to improve the photocatalytic reduction ability of photoelectrodes. Zhang et al. [11] used BiOCl/rGO aerogel as a photocathode to construct a PFC to reduce internal resistance, which indicated a better power generation capacity (696.51 ± 5.27 mV) than that of a single MFC (455.36 ± 7.18 mV). Mahmoodi et al. synthesized graphene oxide (GO)-CTS and AGO-CTS hydrogel adsorbents by mechanical mixing and characterized them using various techniques. The optimal adsorption parameters were pH 5, $C_i$ 100 ppm and dosage 1.5 g/L. The removal rates of GO-CTS and AGO-CTS hydrogel adsorbents were 90.42% and 97.06%, respectively [12]. Hirakawa et al. [13] used several commercially available types of $TiO_2$ with different crystal phases, surface areas, and particle sizes to produce photocatalytic $NH_3$ from water and $N_2$. They found that under environmental conditions, UV radiation of commercially available $TiO_2$ with many surface $Ti_3$ species effectively produced $NH_3$ from water and $N_2$. This substance is the most efficient among the reported powder photocatalysts, but its efficiency is lower than that of natural photosynthesis and artificial photosynthesis. Xu et al. [14] used $TiO_2$ and $SiO_2$ to modify the electrode; next, they irradiated it with UV light and introduced a photocatalytic reaction into the MFC anode chamber to conduct the ammonia nitrogen nitrification reaction, and the cathode chamber performed the denitrification reaction. The system improved the electricity generation performance of the MFC without an extra carbon source. $TiO_2$ has been widely used in photocatalysis, but its utilization efficiency in sunlight is low [15]. $TiO_2$ can only respond to UV light because of its relatively large bandgap. Molybdenum disulfide ($MoS_2$) nanomaterials are easily available, economically feasible, and exhibit satisfactory semiconductor properties [16,17]. The changeable atomic coordination structure and electronic structure of $MoS_2$ make the carrier transmission speed extremely fast, over 200 $cm^2/(V{\cdot}s)$, and its bandgap width is 1.19 to 1.9 eV. These factors make it possess a strong visible light absorption capacity and abundant catalytic active sites [17–20], making it an ideal material for visible light catalytic systems. However, their high surface energy and easy agglomeration limit their development in the field of photocatalysis.

Jaleel UC et al. [21] discussed the geometric structure, polymorphism, preparation methods, and characterization of $MoS_2$-based composites for the photocatalytic degradation of organic dyes. $MoS_2$-based nanomaterials exhibit good degradation activity for organic dyes and toxic pollutants. This research field provides a crucial opportunity for the preparation of excellent photocatalysts that affect the degradation of organic pollutant dyes in wastewater. Thomas et al. [22] discussed the synthesis strategies of 2D $MoS_2$. That $MoS_2$ costs less than the noble metals makes it the cheapest alternative that has been explored for photocatalytic hydrogen production applications. The reactive oxygen species produced by light irradiation of $MoS_2$ can produce oxidative stress on microorganisms, which can be used for water disinfection. GO has a large specific surface area, good flexibility, and good chemical stability. Combining it with $MoS_2$ compensates for the limitations of $MoS_2$ in morphology and other limitations, which can also enhance the photoelectric properties [23].

Dolatabadi et al. [24] synthesized $TiO_2$/ZnO nanostructures by using sol–gel solid-phase dispersion and hydrothermal methods for the degradation of RhB; the degradation test results of all samples showed that although sample $S_1$ synthesized by the sol–gel method had the best degradation effect on RhB, the sample prepared by the hydrothermal method had a better degradation effect on RhB than that. In this study, a composite of GO and $MoS_2$ was prepared using mechanical oscillation and hydrothermal synthesis as a cathode to construct a dual-chamber PFC system. The characterization and electrochemical performance analyses of the composite electrode materials were performed. The ammonia nitrogen removal effect of the system composed of composite materials obtained using different preparation methods was tested, and this result was combined with an analysis of the catalytic performance to optimize the electrode preparation methods. On this basis, oxidation product analysis was performed using quenching denitrification experiments to explore the denitrification mechanism.

## 2. Materials and methods

### 2.1. Composite electrode

The anode consisted of a 2 cm × 2 cm carbon cloth ultrasonically cleaned with $CH_3COCH_3$, $CH_3CH_2OH$, and deionized water. The graphite-based cathode was fabricated using two steps:

#### 2.1.1. GO and $MoS_2$

##### 2.1.1.1. Graphene oxide

$NaNO_3$, $H_2SO_4$, and graphite powder were blended, and $KClO_4$ and $KMnO_4$ were added under ice bath stirring. This mixture was then removed from the ice bath and stirred continuously for 24 h. Deionized water and $H_2O_2$ were added until the solution became bright yellow. The suspension was centrifuged and repeatedly rinsed until it became neutral and vacuum-dried to obtain the GO particles.

##### 2.1.1.2. Molybdenum disulfide

$Na_2MoO_4$ and thiourea were dissolved in deionized water, transferred to a hydrothermal reactor in an oven

(200°C) for 24 h, and cooled to room temperature naturally. The samples were rinsed with deionized water and $CH_3CH_2OH$ repeatedly, centrifuged, filtered, dried, and stored for later use [25].

#### 2.1.2. Cells application: effect of catalyst composition

Three types of electrodes were used.

The electrode sheets used in the cathode were self-made [26].

##### 2.1.2.1. $MoS_2$ electrode

$MoS_2$ was dissolved in deionized water, and a Nafion solution was added. After the ultrasonic treatment, $MoS_2$ was deposited on the surface of the graphite electrode sheet. The sheet was then dried in an oven to obtain the $MoS_2$ electrode.

##### 2.1.2.2. $MoS_2$/GO-MO electrode

$MoS_2$, GO particles, and hexadecyl trimethyl ammonium bromide (CTAB) were placed into deionized water. After thorough mixing by continuously ultrasonic procedure, the mixture was deposited on a graphite electrode in a manner similar to that for the $MoS_2$ electrode. A $MoS_2$/GO-MO electrode was fabricated.

##### 2.1.2.3. $MoS_2$/GO-TH electrode

The GO powder was magnetically stirred in deionized water, and $Na_2MoO_4$ and thiourea were added later. Next, $MoS_2$/GO particles were obtained using the hydrothermal synthesis method. The deposition procedure for the $MoS_2$/GO particles and electrode sheet was then performed. Finally, the $MoS_2$/GO-TH electrode was obtained.

### 2.2. Characterization

In this experiment, an X-ray diffractometer was used to analyze the phases of the samples. The scanning speed was 5°/min, and the range was 5°–80°. The surface morphology of the electrode materials was observed and analyzed using a QuaMa450 (FEI Company, United States). A fluorospectrophotometer (F-4600) was used to measure the lifetime of the photogenerated carriers in the electrode material.

### 2.3. Construction of the PFC system

In this experiment, a 125 mL traditional dual-chamber microbial fuel cell was used. The primary material of the reactor was plexiglass, and *E. coli* was used as the anode electricity-generating bacteria. The catholyte and anolyte (50 mL) were added to the cathode and anode compartments, respectively. The Nafion 117 proton exchange membrane was pretreated by immersion in 5% $H_2O_2$ solution, deionized water, and 5% $H_2SO_4$ solutions to separate the anode and cathode compartments. The preparation process required heating in a constant-temperature water bath at 80°C for 2 h. Subsequently, the Nafion 117 proton exchange membrane was repeatedly rinsed, soaked in deionized water, and stored for later use. In the experiment, $NH_4Cl$ was used to prepare 50 mg/L of ammonia nitrogen simulated wastewater, and a mercury lamp was used as the light source (250 W).

### 2.4. Electrochemical analysis

The polarization curve reflects the relationship between the output voltage and current of the PFC system, which is an evaluation index that characterizes the performance of a battery or electrode [27]. The resistance gradually decreased from the highest value, and the voltage data after each adjustment of a new external resistance was stable for 30 min.

Cyclic voltammetry was used to analyze the electrochemical properties of the working electrode in the PFC system, such as the oxidation–reduction potential, current density, and electron acquisition sensitivity. A LK98B II electrochemical workstation was used to test the redox potential of the prepared working electrode. Under full aeration conditions, the current polarity was set to oxidation, the scan rate was set to 2 mV/S, the scan range was –0.6–1.0 V, and the number of cycles was 10.

### 2.5. Chemical analysis

In this experiment, Nannenberg spectrophotometry was used to determine $NH_4^+$–N, N-(1-naphthalene)-ethylenediamine spectrophotometry was used to determine $NO_2^-$–N, and UV spectrophotometry was used to determine $NO_3^-$–N.

### 2.6. Reaction mechanism analysis

To explore the transformation effect of the PFC system on ammonia nitrogen and compare the effect of the electrode materials, we used an $MoS_2$/GO-TH electrode, an $MoS_2$/GO-MO electrode, and $MoS_2$ electrodes as the cathode of the battery to construct a PFC system for the ammonia nitrogen transformation experiment. Changes in the concentrations of ammonia nitrogen, nitrate, and nitrite were detected during the reaction, and the transformation mechanism according to the transformation products was studied. Except for the influencing factors experiment, the control conditions were pH = 10, an external 20 Ω resistor, an aeration rate of 0.15 $m^3$/h, and an illumination time of 6 h.

To explore the influencing factors, we conducted the experiment in a PFC system that had the best performance in the completed experiments. The influence of the operating conditions, including dissolved oxygen (DO) concentration and pH, on the ammonia nitrogen in the PFC system was investigated. To discuss the effect of DO, we set the pH to 10, and the removal rate of ammonia nitrogen and the generation rate of nitrate and nitrite were explored by controlling the oxygen intake rate to 0.05, 0.1, 0.15, and 0.2 $m^3$/h, respectively. In the pH influencing factor experiment, neutral and alkaline pH are conducive to ammonia oxidation [28], the oxygen intake rate was 0.1 $m^3$/h according to the results of the DO effect experiment, and the transformation regulation of ammonia nitrogen was discussed with the pH of the catholyte adjusted to 6, 8, 10, and 12, respectively.

## 3. Results

### 3.1. Characterization of electrodes

The X-ray diffraction spectrum shown in Fig. 1a shows diffraction peaks at 2θ = 13.38°, 32.44°, 35.02°, and 57.90°, which correspond to the characteristic crystal planes of $MoS_2$ [29,30]. The other two results also have the characteristic diffraction peaks of $MoS_2$; additionally, the diffraction peak of graphene (002) appeared at 2θ = 26.56°, indicating the existence of $MoS_2$ and GO in the composite materials $MoS_2$/GO-TH and $MoS_2$/GO-MO.

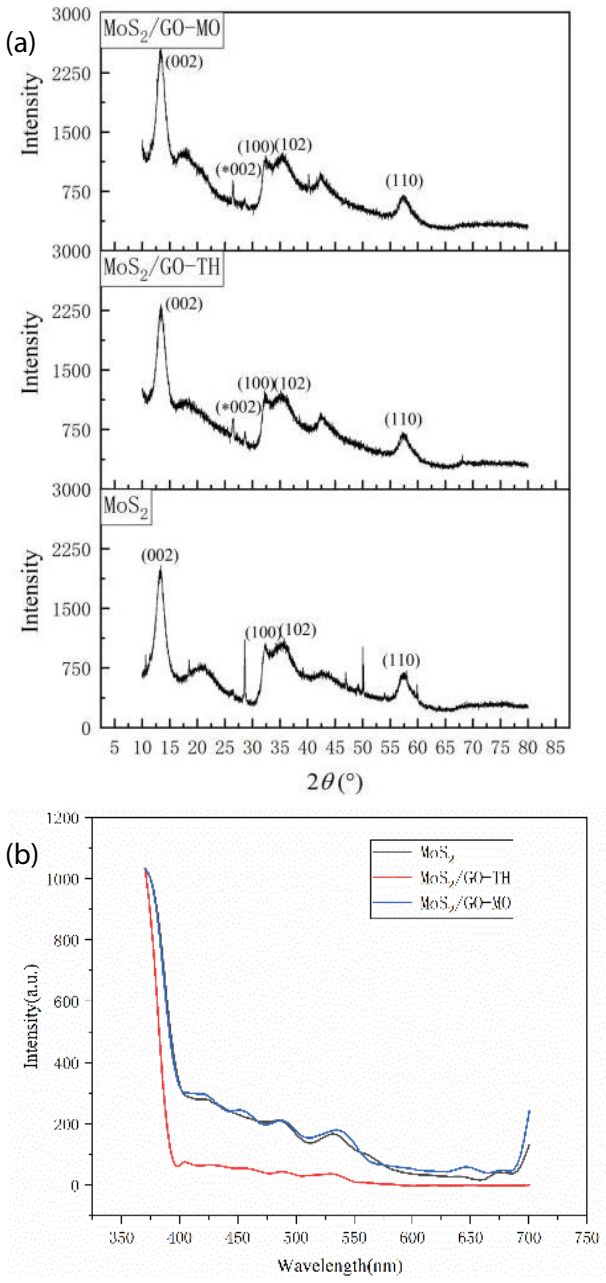


Fig. 1. (a) X-ray diffraction patterns of different electrode materials. (b) Photoluminescence spectra of different electrode materials.

The photoluminescence (PL) spectrum shows the charge recombination and migration efficiency of the material; a lower photoluminescence intensity indicates a lower photoelectron recombination rate [31]. As shown in Fig. 1b, the $MoS_2$ material exhibits a mass of PL peaks in the range of 400–700 nm. Both composite particles, $MoS_2$/GO-MO and $MoS_2$/GO-TH, have smoother spectra than that of $MoS_2$. The results indicate that the addition of GO effectively reduced the PL peak intensity, indicating that the recombination of electron–hole pairs was inhibited. In addition, $MoS_2$/GO-TH barely has peak PL peaks, which indicates that the composite prepared using the hydrothermal synthesis method may be better photocatalytic performance than that of $MoS_2$/GO-MO.

Different electrode materials were scanned using an electron microscope (Fig. 2a and b) show $MoS_2$ with an obviously polymerized flower-like microsphere structure and a particle size of 10–20 μm. A similar agglomerative morphology was obtained for the $MoS_2$ material prepared by Zhang et al. [32], indicating that the $MoS_2$ material was successfully prepared using the hydrothermal method. (c) and (d) are $MoS_2$/GO-TH, and the flower-like microsphere $MoS_2$ particles evenly adhered to the surface of the GO particles to grow. This phenomenon is conducive to the thorough contact between the GO nanoparticles and the $MoS_2$ nanosheets, increasing the specific surface area of the composite material and the photoelectrons-holes transfer efficiency, increasing catalytic efficiency. Next, we compared (a) and (b): the particle size of the $MoS_2$ nanoplatelets grown on the surface of the GO particles was –2–6 μm, which was significantly smaller than that of pure $MoS_2$. This result demonstrates that by growing $MoS_2$ nanosheets on the surface of the GO particles, the agglomeration of the $MoS_2$ nanosheets can be reduced, decreasing the particle size and increasing the uniformity of the distribution. (e) and (f) [33,34] were $MoS_2$/GO-MO, and the results showed that in the composite material prepared using the mechanical oscillation method, the $MoS_2$ nanosheets were rarely scattered on the surface of the GO nanoparticles, and the particle size was between 4 and 6 μm, which is relatively large. The $MoS_2$/GO composite prepared using the hydrothermal synthesis method had more active sites that attracted pollutants than the mechanical oscillation method. In addition, the $MoS_2$ was evenly dispersed and loaded on the GO particles so that carriers could be quickly separated into electrons and holes under the effect of electric potential, accelerate the transfer of electrons, and improve catalytic ability.

### 3.2. Analysis of electrochemical catalytic performance

The polarization curves and power density curves of the three systems showed that the current density increased with an increase in the external resistance, and the power density gradually decreased after increasing to a certain value. The open circuit voltages of the $MoS_2$/GO-TH system, $MoS_2$/GO-MO system, and $MoS_2$ system were 0.49, 0.41, and 0.35 V, respectively, and the maximum power densities were 4.9, 3.82, and 3.29 W/m$^3$, respectively (Fig. 3a). The PFC system with the $MoS_2$/GO composite material as the battery cathode was stronger power generation

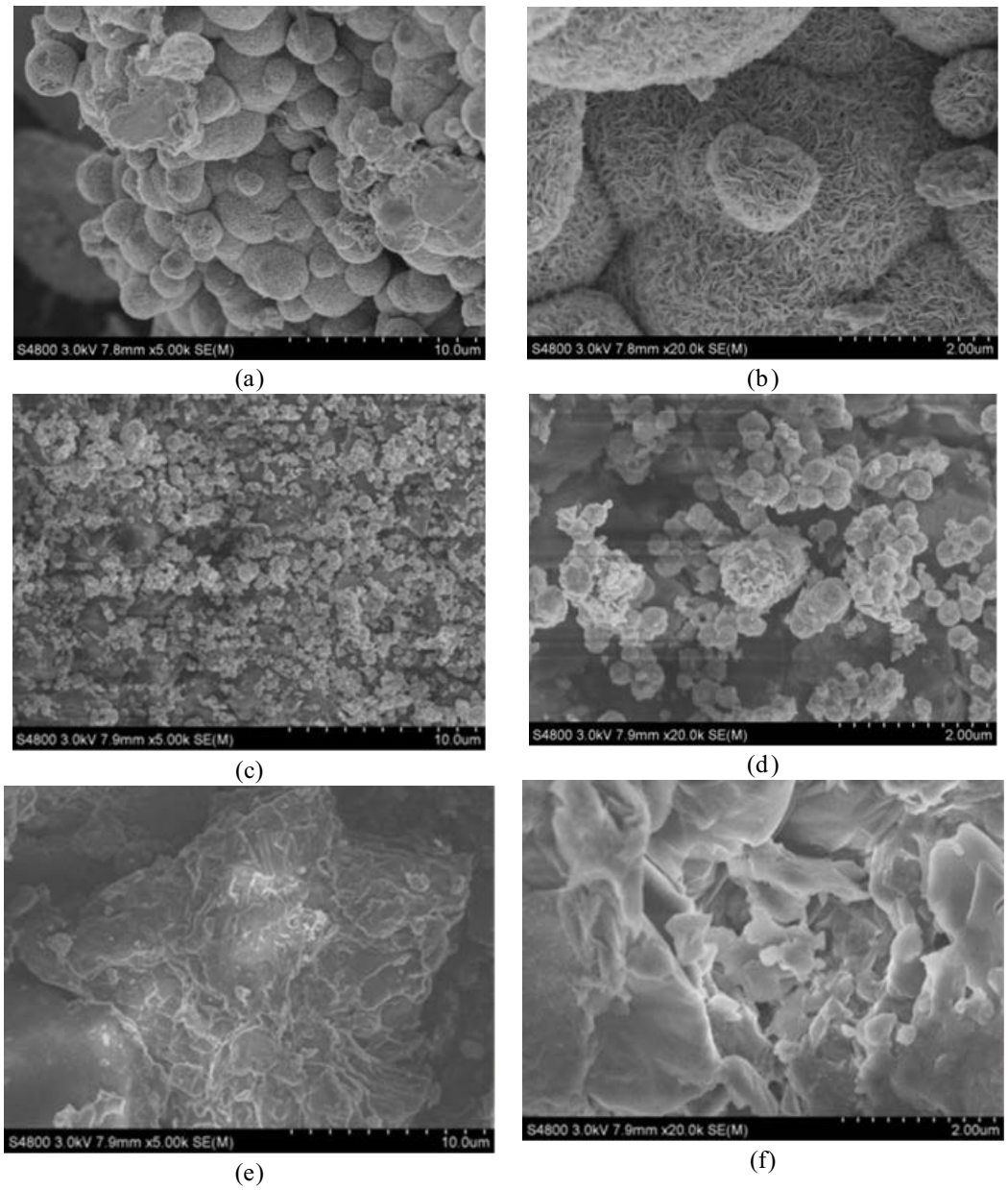


Fig. 2. Scanning electron microscopy results of different electrode materials: (a,b) are $MoS_2$, (c,d) are $MoS_2$/GO-TH composite materials and (e,f) are $MoS_2$/GO-MO composite materials.

capacity than other systems, which can reduce the ohmic loss during the reaction process, to improve degrade ammonia nitrogen.

The cyclic voltammetry curve (Fig. 3b) shows that in the case of oxygen saturation, the three electrode materials all have redox peaks; thus, they all have redox activity. However, the redox peak of $MoS_2$ was not obvious, indicating that its oxidability was not high. The current density of the oxidation potential of the $MoS_2$/GO-TH was 0.42 A/m$^3$, which was higher than that of the $MoS_2$/GO-MO (0.39 A/m$^3$) and the $MoS_2$ (0.30 A/m$^3$). The current density determines the ability of the oxygen to be reduced. The greater the current density, the stronger the ability to reduce oxygen. Therefore, $MoS_2$/GO-TH exhibited better catalytic activity than other systems. Based on the closed curve of each catalytic electrode, the largest area was that of $MoS_2$/GO-TH, indicating that the catalytic effect of the composite was better than those of the other two. Notably, in the cyclic voltammetry curves of the three catalysts, $MoS_2$/GO-TH and $MoS_2$/GO-MO had two oxidation peaks. The additional oxidation peak may be due to the partial reduction of GO in the composite material.

### 3.3. Removal of ammonia nitrogen in the PFC system

The transformation effect of ammonia nitrogen demonstrates that the three systems can effectively degrade ammonia nitrogen (Fig. 4). The transformation efficiencies of the

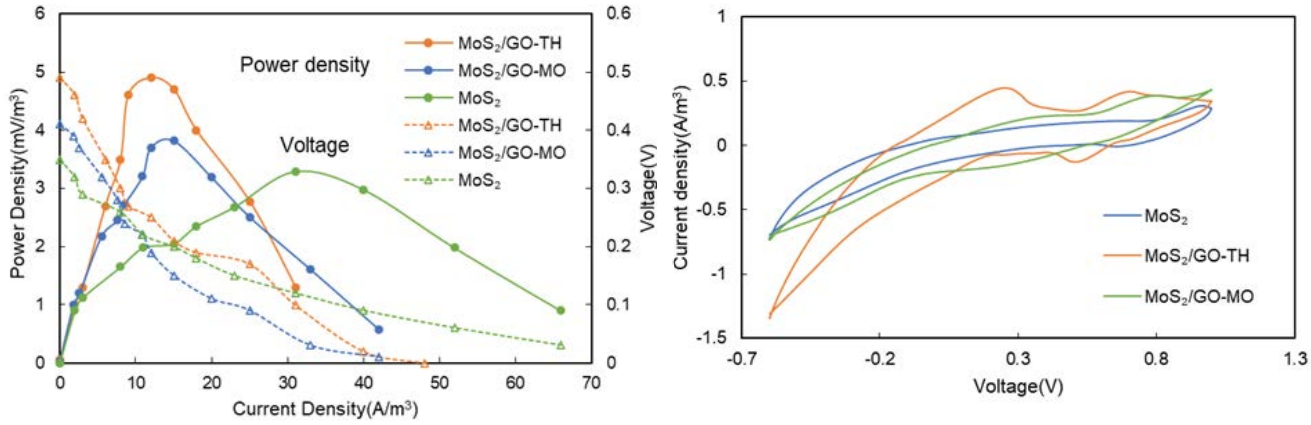


Fig. 3. (a) Polarization curves and power density curves of different electrode materials and (b) CV diagram of different materials.

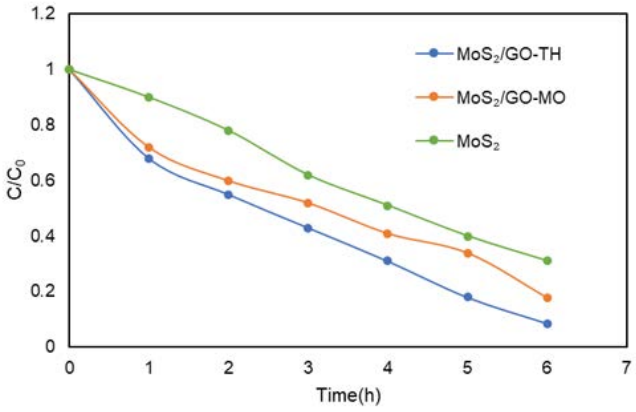


Fig. 4. Transformation effect of different systems on ammonia nitrogen.

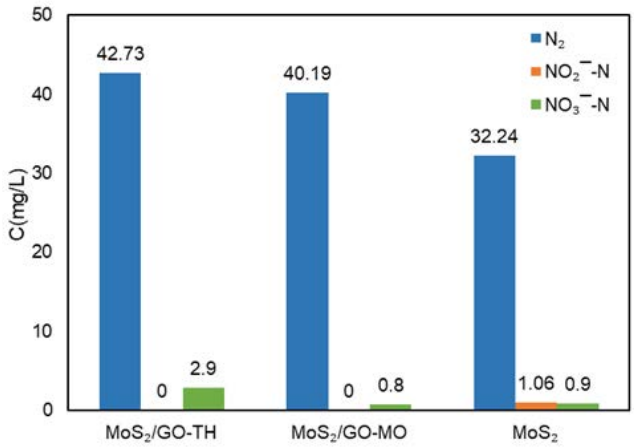


Fig. 5. Ammonia nitrogen transformation under different systems.

$MoS_2$/GO-TH system, the $MoS_2$/GO-MO system, and the $MoS_2$ systems to ammonia nitrogen were 91.4%, 82.1%, and 68.5%, respectively. The $MoS_2$/GO-TH system had the best transformation performance, which might be because the hydrothermal method gave the $MoS_2$/GO electrode more uniform reactive sites, making $MoS_2$ evenly dispersed on the surface of the GO particles [35]. The effective combination of $MoS_2$ and GO particles also inhibited the recombination of electron–hole pairs; thus, $MoS_2$/GO-TH had strong catalytic ability [36].

In the $MoS_2$/GO-TH system, only 5.8% of the ammonia nitrogen was converted to nitrate, no nitrite was produced, and approximately 85.46% of the ammonia nitrogen was converted to nitrogen (Fig. 5). Most of the ammonia nitrogen was successfully converted to nitrogen in the presence of oxygen, and a small portion was converted to nitrate. Almost no nitrite was produced. The photocatalyst was used as the PFC cathode, and the ammonia nitrogen wastewater was transferred to the cathode for treatment, which successfully avoided the mutual conversion of nitrogen-containing compounds among valences. This systems was conducive to the removal of ammonia nitrogen.

### 3.4. Reaction mechanism research

On the basis of these experimental results, the $MoS_2$/GO-TH electrode material with the best effect was used for subsequent experiments.

#### 3.4.1. Effect factors of operating conditions

pH can directly affect the charge distribution on the catalyst surface [37]. During electrochemical ammonia nitrogen oxidation, acidic conditions are conducive to the reduction of nitrate and nitrite [38]. Therefore, the output of by-products, such as nitrate and nitrite, in the solution is low or nonexistent. However, the removal rate of ammonia nitrogen under acidic conditions is significantly lower than that under alkaline conditions [39]. Therefore, what is particularly critical is to make the reaction produce as few by-products as possible, such as nitrate, under alkaline conditions without affecting the removal rate of ammonia nitrogen. The transformation effect of ammonia nitrogen at different pH values demonstrated that the removal rate of

ammonia nitrogen under neutral and partial alkali conditions was significantly lower than that under alkaline conditions (Fig. 6a and b). With an increase in the pH value, the transformation effect of ammonia nitrogen gradually increased, up to 93.8%, but the by-products produced also increased significantly. This phenomenon was observed because, under alkaline conditions, the surface of the $MoS_2$/GO-TH electrode was negatively charged, which was conducive to the generation of •OH free radicals [40]. The removal rate of ammonia nitrogen is improved. In addition, under alkaline conditions, ammonia nitrogen exists in the form of $NH_3$ molecules [41], which is conducive to the enrichment of $NH_3$ molecules on the electrode surface. Notably, when the pH of the solution increased from 10 to 12, although the removal rate of ammonia nitrogen increased, the output of nitrate increased significantly. Therefore, adjusting the pH value of the solution to 10 can achieve a good ammonia nitrogen transformation effect while producing fewer by-products than other pH did.

Increasing the concentration of dissolved oxygen (DO) in the solution can promote the generation of $•O_2^-$ and •OH free radicals to improve the efficiency of the ammonia nitrogen transformation. However, when the concentration of DO in the solution is too high, the generated free radicals further oxidize to produce by-products such as nitrate and nitrite. Therefore, controlling the concentration of DO in the solution is critical for the conversion of nitrogen in the solution. The removal effect of ammonia nitrogen at different DO concentrations is shown in Fig. 6c and d. With a continuous increase in the DO concentration in the solution, the removal rate of ammonia nitrogen increased by 1.41 times to 96.0%. However, although the removal rate of ammonia nitrogen increased, the amount of by-products produced increased. Because of the removal rate of ammonia nitrogen and the amount of by-products generated, the optimal oxygen intake volume should be 0.1 $m^3$/h.

### 3.4.2. Research on transformation path of ammonia nitrogen

In the PFC system, the anode electricity-generating bacteria decomposed the organic carbon source to generate $e^-$ and $h^+$, and the generated electrons were transferred from the battery anode to the battery cathode through the external circuit. When the cathode receives electrons from the anode, the photocatalyst supported on the cathode sheet is irradiated by a mercury lamp to generate photogenerated electron–hole pairs. The photogenerated electrons from the anode react with dissolved oxygen to form

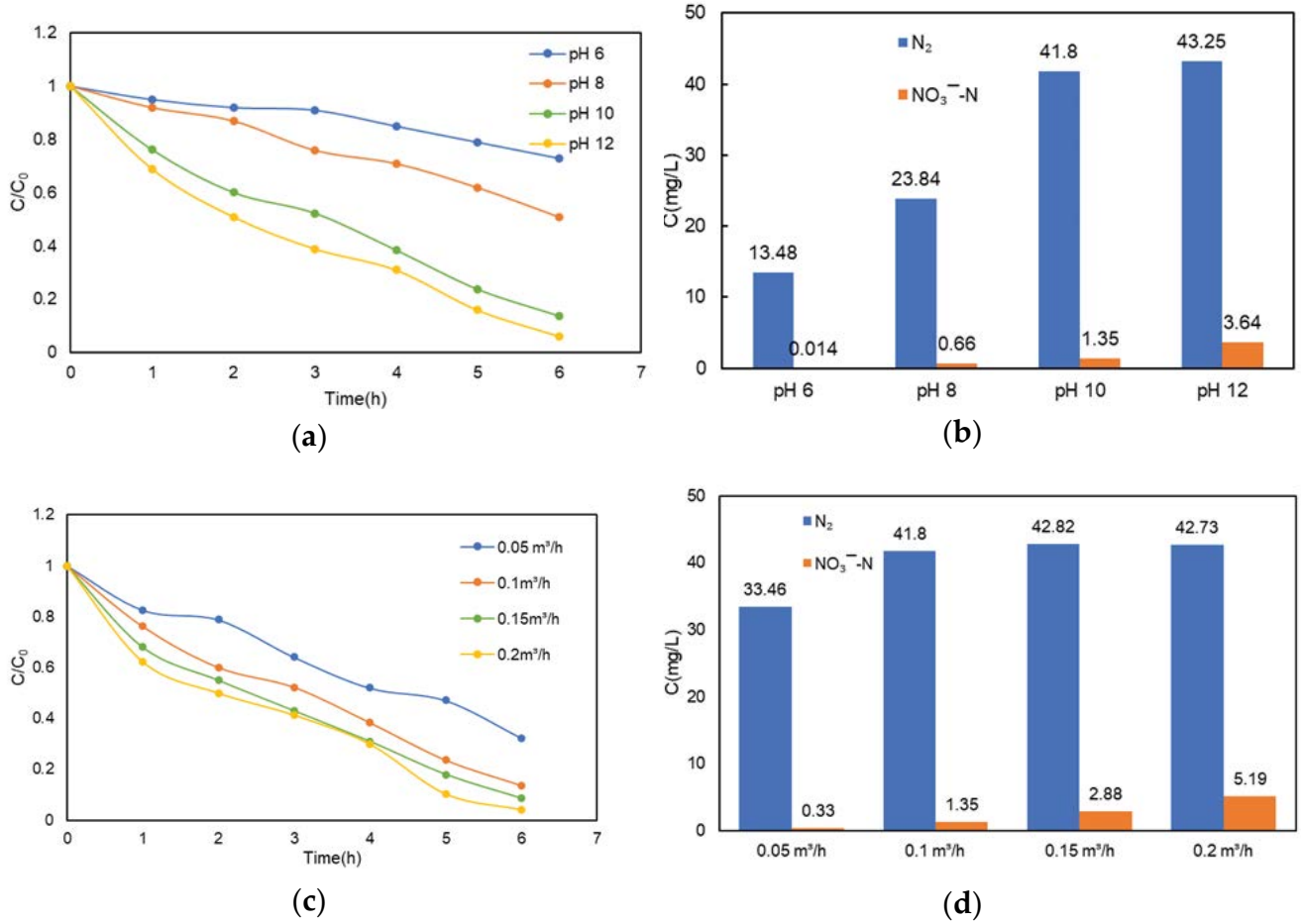


Fig. 6. (a,b) transformation effect of ammonia nitrogen at different pH values and (c,d) removal rate of ammonia nitrogen at different dissolved oxygen concentrations.

highly active oxide species with strong oxidizing properties [42]. Therefore, in the process of the PFC transformation of ammonia nitrogen, the removal of ammonia nitrogen has different oxidation pathways according to the oxide species, which are primarily divided into two aspects: (1) the photocathode electron–hole pairs are separated, and the generated valence band holes directly oxidize ammonia nitrogen, and (2) hydroxyl radicals (•OH) [43–45] or superoxide radicals ($^{\bullet}O_2^-$) [46] are generated for indirect oxidation. In this experiment, KI was selected as the hole trapping agent, $C(CH_3)_3OH$ was selected as the •OH trapping agent, and the transformation mechanism of PFC was explored through a quenching experiment of the oxide species.

After adding the KI reagent to the solution under normal aeration, the ammonia nitrogen transformation effect of the system was not affected, whereas the transformation ability of the photoelectrode in the system without oxygen was significantly inhibited (Fig. 7a). The reason for this phenomenon may be that holes were trapped after adding the KI reagent, which stimulated the separation of electron–hole pairs. In addition, the anode continuously transports electrons to the cathode, generating $^{\bullet}O_2^-$ and •OH radicals to degrade ammonia nitrogen under the action of oxygen.

After adding $C(CH_3)_3OH$, the transformation effect of the system under the anaerobic state was unsatisfactory, and the ability of the system to degrade ammonia nitrogen under normal aeration conditions was not limited (Fig. 7b). The reason for this phenomenon is that •OH radicals were not the main oxides. In addition, the ammonia nitrogen removal rate under aerobic conditions was not significantly affected. This result may have been due to the reaction of $C(CH_3)_3OH$ with •OH radicals in the aerobic state to generate $^{\bullet}O_2^-$ radicals [Eq. (1)], and simultaneously, the dissolved oxygen near the cathode was reduced by electrons to generate $^{\bullet}O_2^-$ radicals. Therefore, the transformation of $C(CH_3)_3OH$ under normal aeration was not affected.

$$C(CH_3)_3OH + {}^{\bullet}OH \rightarrow {}^{\bullet}CH_2(CH_3)_2COH + H_2O_2 \quad (1)$$

*3.4.3. Reaction mechanism speculation*

We studied the transformation products and found that most of the ammonia nitrogen in the system was converted to nitrogen, but a small amount was converted to nitrate nitrogen. By controlling the dissolved oxygen and adding a hole trapping agent and hydroxyl radical trapping agent, the transformation pathway of ammonia nitrogen can be explored. After the addition of KI and $C(CH_3)_3OH$, the transformation effect under the normal aeration state was not inhibited, and the transformation effect under the anaerobic state was not ideal, indicating that oxygen may have been the decisive factor in this experiment and that various oxide species may have been generated during the reaction, resulting in various oxidation pathways. That is, under the irradiation of a mercury lamp, the photocatalyst proposed on the surface was excited by light to generate photogenerated electrons and holes. The photogenerated electrons and the electrons generated by the anode react with oxygen to reduce to $^{\bullet}O_2^-$ radicals; subsequently, the $^{\bullet}O_2^-$ radicals react successively to obtain $H_2O_2$ and •OH radicals. In addition, the holes and various oxide species generated convert ammonia nitrogen into nitrogen gas. This process was accompanied by the production of a small amount of nitrate (Fig. 8). The specific speculation is as follows:

$$e^- + O_2 \rightarrow {}^{\bullet}O_2^- \quad (2)$$

$$^{\bullet}O_2^- + 2H^+ + e^- \rightarrow H_2O_2 \quad (3)$$

$$H_2O_2 + hv \rightarrow {}^{\bullet}OH + OH^- \quad (4)$$

$$^{\bullet}OH + NH_4^+ - N \rightarrow N_2 + H_2O + \text{Nitrogenous by-products}\left(NO_3^- - N/NO_2^- - N\right) \quad (5)$$

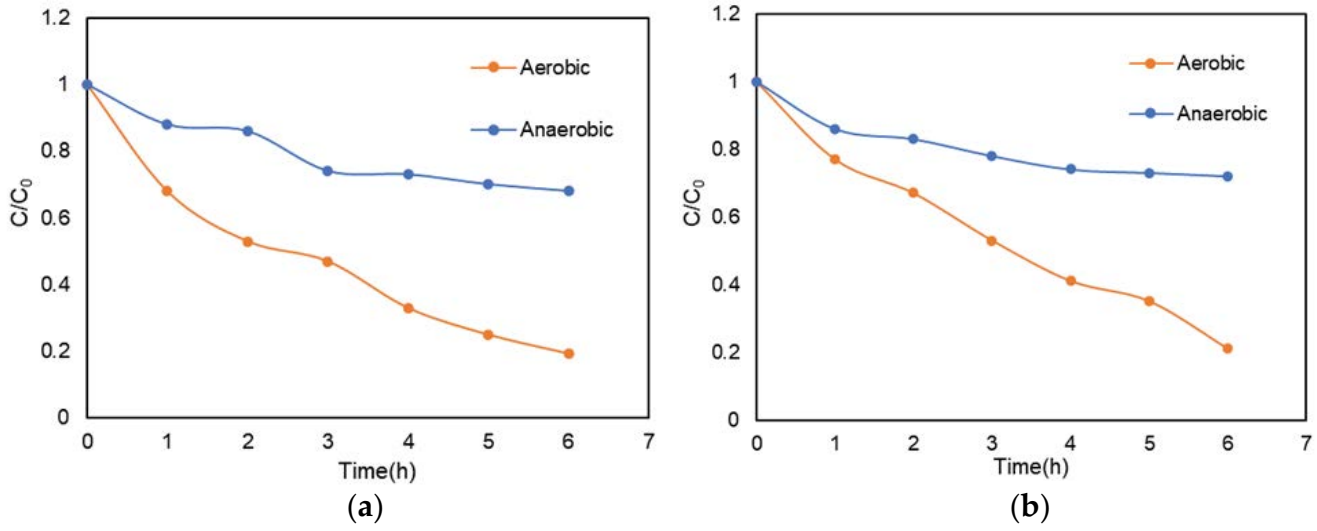


Fig. 7. (a) Influence of KI on transformation effect of photocatalytic fuel cells system and (b) effect of $C(CH_3)_3OH$ on transformation of photocatalytic fuel cells system.

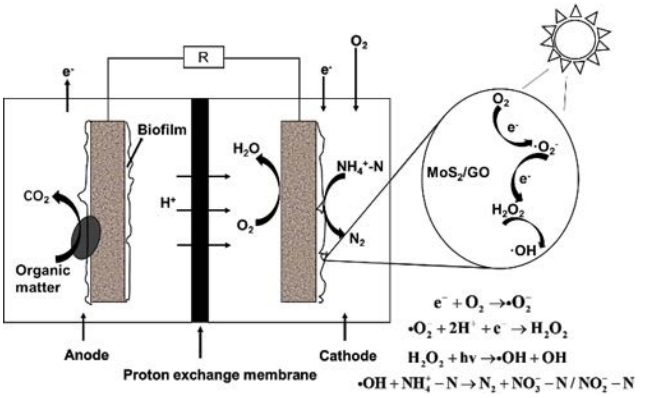


Fig. 8. Transformation reaction mechanism of photocatalytic fuel cells system.

## 4. Conclusion

The $MoS_2$/GO-MO electrode and the $MoS_2$/GO-TH electrodes were fabricated using mechanical oscillation and hydrothermal methods, respectively. Both methods successfully loaded $MoS_2$ nanomaterials with GO particles. The $MoS_2$/GO-TH composite material exhibited a homogeneous distribution of $MoS_2$ on GO, leading to effective inhibition of the recombination of electron–hole pairs. PFC systems with $MoS_2$/GO-MO, $MoS_2$/GO-TH, and $MoS_2$ electrodes were constructed to remove ammonia nitrogen wastewater. Among them, the $MoS_2$/GO-TH system had the largest output voltage, smallest ohmic loss during the reaction, and best redox capability. The removal rate of ammonia nitrogen was as follows: $MoS_2$/GO-TH system > $MoS_2$/GO-MO system > $MoS_2$. Most of the ammonia nitrogen in the three systems was converted into nitrogen, and only a small portion was converted into nitrate and nitrite; the quenching experiment proved that oxygen in the PFC system was the decisive factor; and there were many oxidation paths during the reaction process. The photogenerated electrons and electrons generated by the anode react with oxygen to generate $H_2O_2$ and $^{\bullet}OH$ radicals. The holes and various oxide species generated convert ammonia nitrogen into nitrogen gas.

## Author contributions

Conceptualization, Jing REN and Chunxu HAO; Data curation, Jiyue Zhang, Yao Li, and Na Li; Formal analysis, Rui Hu; Investigation, Jing REN; Methodology, Jiyue Zhang, Yao Li, and Na Li; Writing-original draft, Jiyue Zhang and Maohua Du; Writing-review & editing, Jing REN and Chunxu HAO. All authors have read and agreed to the published version of the manuscript.

## Funding

This research was funded by the Scientific Research Fund of the Liaoning Provincial Education Department (LQN201909) and the Open Project of the State Key Laboratory of Urban Water Resources and Environment (QA202139).

## Conflicts of interest

The authors declare no conflicts of interest.

## References

[1] S. Yan, J. Geng, R. Guo, Y. Du, H. Zhang, Hydronium jarosite activation of peroxymonosulfate for the oxidation of organic contaminant in an electrochemical reactor driven by microbial fuel cell, J. Hazard. Mater., 333 (2017) 358–368.
[2] K. Doudrick, T. Yang, K. Hristovski, P. Westerhoff, Photocatalytic nitrate reduction in water: managing the hole scavenger and reaction by-product selectivity, Appl. Catal., B, 136 (2013) 40–47.
[3] M. Kaneko, J. Nemoto, H. Ueno, N. Gokan, K. Ohnuki, M. Horikawa, R. Saito, T. Shibata, Photoelectrochemical reaction of biomass and bio-related compounds with nanoporous $TiO_2$ film photoanode and $O_2$-reducing cathode, Electrochem. Commun., 8 (2006) 336–340.
[4] X. Wang, J. Hu, Q. Chen, P. Zhang, L. Wu, J. Li, B. Liu, K. Xiao, S. Liang, L. Huang, Synergic degradation of 2,4,6-trichlorophenol in microbial fuel cells with intimately coupled photocatalytic-electrogenic anode, Water Res., 156 (2019) 125–135.
[5] N. Ibrahim, S.K. Kamarudin, L. Minggu, Biofuel from biomass via photo-electrochemical reactions: an overview, J. Power Sources, 259 (2014) 33–42.
[6] K. Iyatani, Y. Horiuchi, S. Fukumoto, M. Takeuchi, M. Anpo, M. Matsuoka, Separate-type Pt-free photofuel cell based on a visible light-responsive $TiO_2$ photoanode: effect of hydrofluoric acid treatment of the photoanode, Appl. Catal., A, 458 (2013) 162–168.
[7] H.-X. Han, C. Shi, L. Yuan, G.-P. Sheng, Enhancement of methyl orange degradation and power generation in a photoelectrocatalytic microbial fuel cell, Appl. Energy, 204 (2017) 382–389.
[8] Q. Wang, J. Xu, Y. Ge, Y. Zhang, H. Feng, Y. Cong, Efficient nitrogen removal by simultaneous photoelectrocatalytic oxidation and electrochemically active biofilm denitrification, Electrochim. Acta, 198 (2016) 165–173.
[9] H.-Y. Cheng, X.-D. Tian, C.-H. Li, S.-S. Wang, S.-G. Su, H.-C. Wang, B. Zhang, H.M.A. Sharif, A.-J. Wang, Microbial photoelectrotrophic denitrification as a sustainable and efficient way for reducing nitrate to nitrogen, Environ. Sci. Technol., 51 (2017) 12948–12955.
[10] Q. Liao, L. Li, R. Chen, X. Zhu, H. Wang, D. Ye, X. Cheng, M. Zhang, Y. Zhou, Respective electrode potential characteristics of photocatalytic fuel cell with visible-light responsive photoanode and air-breathing cathode, Int. J. Hydrogen Energy, 40 (2015) 16547–16555.
[11] J. Zhang, Z. Wang, L. Chu, R. Chen, C. Zhang, S. Toan, D.M. Bagley, J. Sun, S. Dong, M. Fan, Unified photo-electrocatalytic microbial fuel cell harnessing 3D binder-free photocathode for simultaneous power generation and dual pollutant removal, J. Power Sources, 481 (2021) 229133, doi: 10.1016/j.jpowsour.2020.229133.
[12] H. Mahmoodi, M. Fattahi, M. Motevassel, Graphene oxide–chitosan hydrogel for adsorptive removal of diclofenac from aqueous solution: preparation, characterization, kinetic and thermodynamic modelling, RSC Adv., 11 (2021) 36289–36304.
[13] H. Hirakawa, M. Hashimoto, Y. Shiraishi, T. Hirai, Photocatalytic conversion of nitrogen to ammonia with water on surface oxygen vacancies of titanium dioxide, J. Am. Chem. Soc., 139 (2017) 10929–10936.
[14] X. Xu, B. Zhou, F. Ji, Q. Zou, Y. Yuan, Z. Jin, D. Zhao, J. Long, Nitrification, denitrification, and power generation enhanced by photocatalysis in microbial fuel cells in the absence of organic compounds, Energy Fuels, 29 (2015) 1227–1232.
[15] C. Wang, H. Liu, Y. Qu, $TiO_2$-based photocatalytic process for purification of polluted water: bridging fundamentals to applications, J. Nanomater., 2013 (2013) 319637, doi: 10.1155/2013/319637.

[16] S. Liu, S. Huang, Atomically dispersed Co atoms on $MoS_2$ monolayer: a promising high-activity catalyst for CO oxidation, Appl. Surf. Sci., 425 (2017) 478–483.
[17] X. Yang, H. Huang, M. Kubota, Z. He, N. Kobayashi, X. Zhou, B. Jin, J. Luo, Synergetic effect of $MoS_2$ and g-$C_3N_4$ as cocatalysts for enhanced photocatalytic $H_2$ production activity of $TiO_2$, Mater. Res. Bull., 76 (2016) 79–84.
[18] J. Schornbaum, B. Winter, S.P. Schießl, F. Gannott, G. Katsukis, D.M. Guldi, E. Spiecker, J. Zaumseil, Epitaxial growth of PbSe quantum dots on $MoS_2$ nanosheets and their near-infrared photoresponse, Adv. Funct. Mater., 24 (2014) 5798–5806.
[19] J. Guo, F. Li, Y. Sun, X. Zhang, L. Tang, Oxygen-incorporated $MoS_2$ ultrathin nanosheets grown on graphene for efficient electrochemical hydrogen evolution, J. Power Sources, 291 (2015) 195–200.
[20] Y. Min, G. He, Q. Xu, Y. Chen, Dual-functional $MoS_2$ sheet-modified CdS branch-like heterostructures with enhanced photostability and photocatalytic activity, J. Mater. Chem. A, 2 (2014) 2578–2584.
[21] J.R. Jaleel UC, R. Madhushree, K.R. Sunaja Devi, D. Pinheiro, M.K. Mohan, Structural, morphological and optical properties of $MoS_2$-based materials for photocatalytic degradation of organic dye, Photochem, 2 (2022) 628–650.
[22] N. Thomas, S. Mathew, K.M. Nair, K. O'Dowd, P. Forouzandeh, A. Goswami, G. McGranaghan, S.C. Pillai, 2D $MoS_2$: structure, mechanisms, and photocatalytic applications, Mater. Today Sustainability, 13 (2021) 100073, doi: 10.1016/j.mtsust.2021.100073.
[23] Y. Fu, H. Chen, X. Sun, X. Wang, Combination of cobalt ferrite and graphene: high-performance and recyclable visible-light photocatalysis, Appl. Catal., B, 111 (2012) 280–287.
[24] S. Dolatabadi, M. Fattahi, M. Nabati, Solid state dispersion and hydrothermal synthesis, characterization and evaluations of $TiO_2$/ZnO nanostructures for degradation of Rhodamine B, Desal. Water Treat., 231 (2021) 425–435.
[25] M. Li, J. Zhou, Y.-G. Bi, S.-Q. Zhou, C.-H. Mo, Transition metals (Co, Mn, Cu) based composites as catalyst in microbial fuel cells application: the effect of catalyst composition, Chem. Eng. J., 383 (2020) 123152, doi: 10.1016/j.cej.2019.123152.
[26] J. Ren, H. Li, N. Li, Y. Song, J. Chen, L. Zhao, A three-dimensional electrode bioelectrochemical system for the advanced oxidation of p-nitrophenol in an aqueous solution, RSC Adv., 10 (2020) 17163–17170.
[27] B. Kokabian, R. Smith, J.P. Brooks, V.G. Gude, Bioelectricity production in photosynthetic microbial desalination cells under different flow configurations, J. Ind. Eng. Chem., 58 (2018) 131–139.
[28] L. Li, Y. Liu, Ammonia removal in electrochemical oxidation: mechanism and pseudo-kinetics, J. Hazard. Mater., 161 (2009) 1010–1016.
[29] A.M.A. Omar, A. Hassen, O.I. Metwalli, M.R. Saber, S.R.E. Mohamed, A.S.G. Khalil, Construction of 2D layered $TiO_2$@$MoS_2$ heterostructure for efficient adsorption and photodegradation of organic dyes, Nanotechnology, 32 (2021) 335605, doi: 10.1088/1361-6528/abff8a.
[30] M.R. Saber, G. Khabiri, A.A. Maarouf, M. Ulbricht, A.S.G. Khalil, A comparative study on the photocatalytic degradation of organic dyes using hybridized 1T/2H, 1T/3R and 2H $MoS_2$ nano-sheets, RSC Adv., 8 (2018) 26364–26370.
[31] L. Xu, L. Yang, E.M. Johansson, Y. Wang, P. Jin, Photocatalytic activity and mechanism of bisphenol a removal over $TiO_{2-x}$/rGO nanocomposite driven by visible light, Chem. Eng. J., 350 (2018) 1043–1055.
[32] X. Zhang, X. Huang, M. Xue, X. Ye, W. Lei, H. Tang, C. Li, Hydrothermal synthesis and characterization of 3D flower-like $MoS_2$ microspheres, Mater. Lett., 148 (2015) 67–70.
[33] X. Hou, Z. Wang, G. Fan, H. Ji, S. Yi, T. Li, Y. Wang, Z. Zhang, L. Yuan, R. Zhang, J. Sun, D. Chen, Hierarchical three-dimensional $MoS_2$/GO hybrid nanostructures for triethylamine-sensing applications with high sensitivity and selectivity, Sens. Actuators, B, 317 (2020) 128236, doi: 10.1016/j.snb.2020.128236.
[34] G. Deokar, D. Vignaud, R. Arenal, P. Louette, J.-F. Colomer, Synthesis and characterization of $MoS_2$ nanosheets, Nanotechnology, 27 (2016) 075604, doi: 10.1088/0957-4484/27/7/075604.
[35] Y. Lv, H. Pan, J. Lin, Z. Chen, Y. Li, H. Li, M. Shi, R. Yin, S. Zhu, One-pot hydrothermal approach towards 2D/2D heterostructure based on 1T $MoS_2$ chemically bonding with GO for extremely high electrocatalytic performance, Chem. Eng. J., 428 (2022) 132072, doi: 10.1016/j.cej.2021.132072.
[36] X. Li, S. Guo, W. Li, X. Ren, J. Su, Q. Song, A.J. Sobrido, B. Wei, Edge-rich $MoS_2$ grown on edge-oriented three-dimensional graphene glass for high-performance hydrogen evolution, Nano Energy, 57 (2019) 388–397.
[37] W. Li, S. Zhang, G. Chen, Y. Hua, Simultaneous electricity generation and pollutant removal in microbial fuel cell with denitrifying biocathode over nitrite, Appl. Energy, 126 (2014) 136–141.
[38] E. Lacasa, P. Cañizares, J. Llanos, M.A. Rodrigo, Removal of nitrates by electrolysis in non-chloride media: effect of the anode material, Sep. Purif. Technol., 80 (2011) 592–599.
[39] Y. Yang, H. Liu, The mechanisms of ozonation for ammonia nitrogen removal: an indirect process, J. Environ. Chem. Eng., 10 (2022) 108525, doi: 10.1016/j.jece.2022.108525.
[40] C. Yin, T. Ye, Y. Yu, W. Li, Q. Ren, Detection of hydroxyl radicals in sonoelectrochemical system, Microchem. J., 144 (2019) 369–376.
[41] D.E. Kissel, M. Cabrera, S. Paramasivam, Ammonium, Ammonia, and Urea Reactions in Soils, J.S. Schepers, W.R. Raun, Eds., Nitrogen in Agricultural Systems, Agronomy Monographs, Vol. 49, 2008, pp. 101–155. Available at: https://doi.org/10.2134/agronmonogr49.c4
[42] H.-Y. Ma, L. Zhao, L.-H. Guo, H. Zhang, F.-J. Chen, W.-C. Yu, Roles of reactive oxygen species (ROS) in the photocatalytic degradation of pentachlorophenol and its main toxic intermediates by $TiO_2$/UV, J. Hazard. Mater., 369 (2019) 719–726.
[43] Y. Liu, J. Xie, C.N. Ong, C.D. Vecitis, Z. Zhou, Electrochemical wastewater treatment with carbon nanotube filters coupled with *in-situ* generated $H_2O_2$, Environ. Sci. Water Res. Technol., 1 (2015) 769–778.
[44] D. Raptis, A. Ploumistos, E. Zagoraiou, E. Thomou, M. Daletou, L. Sygellou, D. Tasis, P. Lianos, Co-N doped reduced graphene oxide as oxygen reduction electrocatalyst applied to photocatalytic fuel cells, Catal. Today, 315 (2018) 31–35.
[45] K. Zhao, J. Bai, Q. Zeng, Y. Zhang, J. Li, L. Li, L. Xia, B. Zhou, Efficient wastewater treatment and simultaneously electricity production using a photocatalytic fuel cell based on the radical chain reactions initiated by dual photoelectrodes, J. Hazard. Mater., 337 (2017) 47–54.
[46] M. Li, Y. Liu, L. Dong, C. Shen, F. Li, M. Huang, C. Ma, B. Yang, X. An, W. Sand, Recent advances on photocatalytic fuel cell for environmental applications—the marriage of photocatalysis and fuel cells, Sci. Total Environ., 668 (2019) 966–978.